Commun. Theor. Phys. **58** (2012) 165–170 Vol. 58, No. 1, July 15, 2012

A Unified Spatio-Temporal Framework of the Cuerno–Barabasi Stochastic Continuum Model of Surface Sputtering

Oluwole Emmanuel Oyewande*

Department of Physics, University of Ibadan, Ibadan, Nigeria

(Received November 7, 2011; revised manuscript received February 29, 2012)

Abstract *The nonlinear continuum model proposed by Cuerno and Barabasi is the most successful and widely acceptable theoretical description of oblique incidence ion sputtered surfaces to date and is quite robust in its predictions of the time evolution and scaling of interfaces driven by ion bombardment. However, this theory has thus far predicted only ripple topographies and rough surfaces for short and large scales, respectively. As a result, its application to the interpretation and study of nanodots, predicted by Monte Carlo simulations for, and observed in experiments of, oblique incidence sputtering is still unclear and, hence, an open problem. In this paper, we provide a new insight to the theory, within the same length scale, that explains nanodot formation on off-normal incidence sputtered surfaces, among others, and propose ways of observing the predicted topographies of the MC simulations, as well as possible control of the size of the nanodots, in the framework of the Cuerno–Barabasi continuum theory.*

PACS numbers: 68.35.-p, 05.10.-a, 79.20.-m
Key words: topographic phase diagrams, surface nanostructures, surface nanodots, Cuerno–Barabasi model

1 Introduction

For some time now a lot of interest has been generated by the ordering behaviour exhibited by surfaces sputtered by energetic ions in which ordered patterns are not only formed in the process of a random ejection of surface particles, but that the orientation of the patterns can be tuned by varying the experimental sputtering parameters.[1−7] Coupled with their nature as nanostructures, these nanopatterns are of technological importance in opto-electronic and other nano-device applications. According to the Cuerno and Barabasi nonlinear continuum theory (CB model), their large length scale characteristics result from nonlinear effects and the sputter noise in the sputtering process.[5−6]

While this defines new scaling regimes absent from the linear theory of Bradley and Harper,[2] as well as ripple topographic regimes agreeing with the linear theory, a number of unresolved problems persist. For instance, the scaling properties of the different scaling regimes are unknown. Furthermore, the nonlinear theory, like the linear theory, has thus far predicted mainly ripple topography at short length scales. Meanwhile, a number of experiments of normal incidence sputtering have demonstrated the existence of a different kind of surface morphology, dot topographies, on semiconductor and amorphous surfaces at nanometre length scales with the presence of a characteristic length scale in the system.[8−9] Moreover, recent Monte Carlo simulations[10−11] reported the existence of these dot topographies for off-normal incidence sputtering of amorphous substrates at collision cascade parameters different from the existing continuum theory calculations. In the simulations,[10] six different topographic regions were reported for early times in the sputtering process. When considering the topographies at later times as well as the nature of the nanostructures, these six regions reduce to three through a merger of four of the regions into one.

Although, a number of targeted theoretical descriptions focussed at accounting for nanodot characteristics have been proposed,[12−14] the actual formation of these nanodots from oblique incidence sputtering remain unclear and is not yet understood, since the CB model has so far not predicted anything other than ripple topographies for off-normal incidence. Moreover, the Continuum theory calculations of the CB model are usually performed for isotropic distribution of the energy of the impinging ion, mainly for ease of exposition of the theory, and a few cases of anisotropic energy distribution that are irrelevant to the nanodot regions of the Monte Carlo simulations. Thus, the continuum theory results so far are inconclusive for certain important cases as enumerated above and below.

We investigate this open problem by providing phase diagram calculations of the continuum theory over a range of collision cascade parameters corresponding to an anisotropic distribution of the energy of the impinging ions. In particular, we provide those necessary to resolve the unanswered questions about the prediction of the continuum theory as regards non-ripple morphologies. We propose a different interpretation of the continuum theory which indicates that for certain anisotropic distribution of

*E-mail: eoyewande@gmail.com

the energy of the impinging ions, the presence of a characteristic length scale may be regarded as a manifestation of the separation between dots and not ripple crests or troughs. We discuss the accessibility of any of the regions studied to experimental probing; propose an explanation for the formation of the dots that arise from oblique incidence ion sputtering and a possible way of achieving or controlling required dot size. The rest of this paper is organized as follows. In the next section we discuss the theory. In Sec. 3, we present and discuss our results for the anisotropic cases relevant to an explanation of yet unaccounted topographies, and provide a new insight to the theory which explains the results. Finally, we provide a brief conclusion in Sec. 4.

2 Materials and Methods

The continuum theoretical description of interface morphology in terms of deterministic and stochastic partial differential equations is a powerful and successful tool for understanding the behaviour of diverse interface phenomena. For the specific case of ion sputtered surfaces, the distribution $E(\boldsymbol{x})$ of the energy E of the incident ion to a surface particle located at position $\boldsymbol{x} = (x_1, x_2, x_3)$ is assumed to be of the Gaussian form:[15]

$$E(\boldsymbol{x}) = \frac{E}{(\sqrt{2\pi})^3 \alpha \rho^2} \exp\Big(- \frac{{x_3}^2}{2\alpha^2} - \frac{{x_1}^2 + {x_2}^2}{2\rho^2} \Big) , \quad (1)$$

where α and ρ are the widths of the distribution parallel and perpendicular to the ion beam direction, respectively. The erosion velocity $\upsilon \propto \partial_t h$ by definition, following which the dynamic evolution of the surface height $h(\boldsymbol{x}, t)$ at nanometre length scales is for most cases governed by the Cuerno-Barabasi model which is a Kuramoto–Sivashinsky type stochastic partial differential equation[2,5]

$$\begin{aligned} \partial_t h(\boldsymbol{x}, t) = & -\upsilon_0 + \zeta \partial_x h(\boldsymbol{x}, t) + \varsigma_x \partial_{xx} h(\boldsymbol{x}, t) \\ & + \varsigma_y \partial_{yy} h(\boldsymbol{x}, t) + \eta_x [\partial_x h(\boldsymbol{x}, t)]^2 \\ & + \eta_y [\partial_y h(\boldsymbol{x}, t)]^2 - D \nabla^4 h(\boldsymbol{x}, t) + \beta , \end{aligned} \quad (2)$$

υ_0 is the erosion velocity of a flat surface, ζ is a proportionality constant related to the local surface slope along the x-direction, ς_x and ς_y are the (linear) surface tension coefficients, η_x and η_y are the nonlinear coefficients, D is the surface diffusion coefficient, β is a (Gaussian) noise term with zero mean, representing the randomness in the ejection of the surface constituents.

Using the convenient notation,

$$\begin{aligned} & a_\alpha = \frac{a}{\alpha} , \quad a_\rho = \frac{a}{\rho\kappa} = \cos\theta , \quad \sigma = \sin\theta , \\ & \varpi = a_\alpha^2 \sigma^2 + a_\rho^2 \kappa^2 , \\ & \Upsilon = \frac{FEPa}{\alpha\rho\sqrt{2\pi\varpi}} \exp\Big(- \frac{a_\alpha^2 a_\rho^2 \kappa^2}{2\varpi} \Big) , \end{aligned}$$

where F is the ion flux and P is the proportionality constant between the power deposition and the rate of erosion, we provide the (Cuerno–Barabasi) coefficients,[5–6] for ease of reference, as follows:

$$\varsigma_x = \Upsilon a \frac{a_\alpha^2}{2\varpi^3} (2 a_\alpha^4 \sigma^4 - a_\alpha^4 a_\rho^2 \sigma^2 \kappa^2 + a_\alpha^2 a_\rho^2 \sigma^2 \kappa^2 - a_\rho^4 \kappa^4) , \quad (3)$$

$$\varsigma_y = -\Upsilon a \frac{\kappa^2 a_\sigma^2}{2\varpi} , \quad (4)$$

$$\begin{aligned} \eta_x = & \Upsilon \frac{\kappa}{2\varpi^4} [a_\alpha^8 a_\rho^2 \sigma^4 (3 + 2\kappa^2) + 4 a_\alpha^6 a_\rho^4 \sigma^2 \kappa^4 \\ & - a_\alpha^4 a_\rho^6 \kappa^4 (1 + 2\sigma^2)] - \varpi^2 [2 a_\alpha^4 \sigma^2 - a_\alpha^2 a_\rho^2 (1 + 2\sigma^2)] \\ & - a_\alpha^8 a_\rho^4 \sigma^2 \kappa^2 - \varpi^4 , \end{aligned} \quad (5)$$

$$\eta_y = \Upsilon \frac{\kappa}{2\varpi^2} (a_\alpha^4 \sigma^2 + a_\alpha^2 a_\rho^2 \kappa^2 - a_\alpha^4 a_\rho^2 \kappa^2 - \varpi^2) . \quad (6)$$

If non-linear effects are irrelevant at the short nano scales of pattern formation Eq. (2) predicts the presence of a characteristic length scale $\Gamma = \sqrt{D/|\varsigma|}$ in the system,[2,5] which manifests as periodic structures (e.g. in the separation of ripple crests/troughs); where $|\varsigma|$ is the higher absolute value of the negative surface tension coefficients, and the structures are oriented along the direction that corresponds to the higher $|\varsigma|$. Thus, if neither of ς_x and ς_y is less than zero, the characteristic length scale is absent and since the ripple wavelength is $\lambda = 2\pi\Gamma\sqrt{2}$ no ripples are formed. In other words, the present continuum theory interpretation is that we either have ripples or not for oblique incidence, whereas reports of other topographies have emerged.

In order to clarify this we obtained the phase diagrams of the continuum theory for the asymmetric energy distribution cases $\alpha = 0$–5 and $\rho = 0$–5 studied in recent reports[10–11] of Monte Carlo simulations of surface sputtering in which atomistic simulations[16] of the range of ions in solids were performed to determine the realistic ranges of collision cascade parameters used in the MC simulations. Our results are presented and discussed in the next section.

3 Results and Discussion

The phase diagrams presented here have been obtained from the variations of ς_x, ς_y, η_x, η_y as functions of α and ρ (Fig. 1); and as functions of a and θ (Fig. 2). From these calculations we found three topographic regions, for $a = 6.0$ and $\theta = 50^\circ$ [Fig. 1(a)], as in the simulations at later times. Since these coefficients are also functions of a and θ it is necessary to obtain the phase diagram in these regard as well. As we show below, the phase diagram in terms of a and θ allow for a wide range of possibilities of the coefficients and a large number of topographic regions. The regions to be encountered below in any of the two cases are as defined in Table 1, where we tabulate the signs of the coefficients defining each region. As will be seen in what follows, if we ignore the nonlinear coefficients then there are only three possible regions, two of which describe ripples with either of the two possible orientations and the remaining one describing the rare sit-

uation in which neither of the surface tension coefficients is negative.

Table 1 Definition of the regions found in the calculations, as described in the text.

Region	Signs of the coefficients
1	$\varsigma_x < \varsigma_y \leq 0$; $\eta_x < 0$, $\eta_y < 0$
2	$\varsigma_y < \varsigma_x \leq 0$; $\eta_x < 0$, $\eta_y < 0$
3	$\varsigma_x < \varsigma_y \leq 0$; $\eta_x > 0$, $\eta_y < 0$
4	$\varsigma_y < \varsigma_x \leq 0$; $\eta_x > 0$, $\eta_y < 0$
5	$\varsigma_x < \varsigma_y \leq 0$; $\eta_x < 0$, $\eta_y > 0$
6	$\varsigma_y < \varsigma_x \leq 0$; $\eta_x < 0$, $\eta_y > 0$
7	$\varsigma_x < \varsigma_y \leq 0$; $\eta_x > 0$, $\eta_y > 0$
8	$\varsigma_y < \varsigma_x \leq 0$; $\eta_x > 0$, $\eta_y > 0$
9	$\varsigma_x > 0$, $\varsigma_y < 0$; $\eta_x > 0$, $\eta_y < 0$
10	$\varsigma_x > 0$, $\varsigma_y < 0$; $\eta_x < 0$, $\eta_y < 0$
11	$\varsigma_x > 0$, $\varsigma_y < 0$; $\eta_x > 0$, $\eta_y > 0$
12	$\varsigma_x > 0$, $\varsigma_y < 0$; $\eta_x > 0$, $\eta_y = 0$

Until now phase diagram calculations have not been done for the range of collision cascade parameters considered in this work and the only continuum theory interpretation of the results of applications of Eq. (2) to an understanding of the time evolution of sputtered surfaces is one that merges two different length scales, one short and the other long; the difference having a lower limit of the order of about 10 μm. While this interpretation is crucial for an understanding of the transition of the surface topography between these length scales as well as the scaling behavior reported by diverse experiments at different length scales, it is difficult to relate it to the occurrence of different morphologies within the same length scale.

In this paper, we provide the results of calculations for these ranges of collision cascade parameters and on their basis propose another interpretation of the result of an application of Eq. (2) within the same length scale, which explains the different possible surface morphologies; for instance, it accounts for the unexplained phenomenon of oblique incidence dot formation. Note that dot pattern formation was associated with normal incidence sputtering until the work of Bradley[17] and Frost[18] who showed that the nanodots occur for oblique incidence sputtering with sample rotation. In Ref. [10] it was shown that the influence of the sample rotation is to purify the dots, as they also occur without sample rotation under certain sputtering conditions, albeit with other underlying periodic and rough structures. It was further shown[10] that these nanodots have very similar characteristics as the normal incidence nanodots.

The normal incidence dot pattern formation on GaSb and InP surfaces is believed to originate from the preferential sputtering and segregation of the surface-rich species,[19−20] while impurity effects play a very important role for dots formed on silicon surfaces.[21−26] Here (see below), we provide an explanation of oblique incidence dot formation based on the Cuerno–Barabasi model which is the applicable model to off-normal incidence sputtered surfaces.

In the phase diagram presented in Fig. 1(a), ripples are oriented along the y-axis in the three regions 2, 4, and 9, whereas, in the simulation ripples are oriented perpendicular to the ion beam direction for the same sputtering parameters. Assuming that the projection of the ion beam direction in the simulation corresponds, in the reference frame of the continuum theory, to a straight line segment parallel to the x-axis, we have an agreement between the continuum and the discrete theories that enables us to interpret the results of the continuum theory as regards dot topographies. For instance, since the disagreement here is in the topography of region 9, then the nonlinear coefficients must be dominant and we explain their role below.

Note that the values of the collision cascade parameters at the phase boundaries are slightly different to those in the simulation results. To investigate this we perform calculations for the phase diagram at different θ [see Figs. 1(b) and 1(c)] and observe shifts in these boundaries, which indicate a quantitative agreement with the values reported in the simulation. The general result for the three regions of Fig. 1(a), when considering both a and θ are shown in Figs. 2(a)–2(c) for $\alpha = 3.3$, $\rho = 4.5$; $\alpha = 1.6$, $\rho = 3.3$; and $\alpha = 2.0$, $\rho = 1.0$, respectively.

A transition from region 2 to 4 of Fig. 1(a), when considering a fixed α and varying ρ, is due to the change of sign of the nonlinear coefficient η_x associated with increasing local surface slopes along the x-axis, which is a precursor to the change from region 4 to 9, in which case there is no directional change in nonlinearity but only a change of sign of the surface tension coefficient ς_x. This is important as it provides an explanation of dot formation which we propose as follows.

A negative surface tension coefficient is representative of the instability arising from the sputtering process in which troughs are eroded in preference to crests.[2] A positive surface tension coefficient then implies a preferential neglect of troughs in the erosion process. On the other hand, a negative nonlinear coefficient implies that the height evolution increases as local surface slopes increase, and vice-versa. This means that the interplay that leads to ripple formation is enhanced or countered depending on the relative signs of the nonlinear coefficients which are capable of creating a further instability that disturbs the interplay. On this basis pattern formation in the twelve regions highlighted above are as tabulated in Table 2 below.

Due to the interplay between ς_x and ς_y, periodic structures with either of two possible orientations are always present, except if one of ς_x or ς_y is zero. Details of how to calculate the characteristic quantities (e.g. ripple amplitude, growth rate, etc.) of the nanostructures in Table 2

can be found in the literature.[6] Some regions of orthogonally oriented ripple structures such as region 1, 2, and 6 in the phase diagram are in agreement with what has been observed by experiments, e.g. Refs. [27–28], that two perpendicular ripple patterns overlaying each other are developed simultaneously on amorphous semiconductor surfaces during ion sputtering at moderate temperature.

Table 2 Description of the nano-patterns characteristic of the regions found in the calculations, as explained in the text.

Region	Description of the nanopatterns
1	Ripples oriented along x with much less prominent underlying periodic structure along y
2	Ripples oriented along y with much less prominent underlying periodic structure along x
3	Ripples oriented along x with shorter amplitude and (possibly prominent, depending on the relative size of ς_y) periodic structure along y
4	Almost pure ripples (i.e. very little or no sign of an underlying periodic structure) oriented along y with normal amplitude growth
5	Almost pure ripples oriented along x with normal amplitude growth
6	Ripples oriented along y with shorter amplitude and (possibly prominent, depending on the relative size of ς_x) periodic structure along x
7	Possibly a rough surface, or low amplitude ripples oriented along x; depending on the relative strengths of the competing factors
8	Ripples oriented along y with slow or no amplitude growth; or rough surface if the nonlinearities cancel out or soften the surface tension instability
9	Dots with underlying periodic structure oriented along y
10	Short ripples oriented along y, or dots of lower growth rate and underlying structure oriented along y; depending or the relative strengths of the competing factors
11	Ripples oriented along x with slow or no amplitude growth; or rough surface if the nonlinearities cancel out or soften the surface tension instability
12	Dots with less prominent or no underlying periodic structure

In particular, we can explain region 9 as follows. Trough erosion along the x-axis is not favored in this case and the height evolution along the x-axis decreases. Since erosion is a stochastic process and erosion along the x-axis for this region is much reduced in comparison to that along the y-axis, the continuity of eroded troughs along the y-axis is broken and instead of long grooves we have pits interspersed with isolated protrusions which together make dot topography. Based on this explanation, dot size depends on the relative magnitudes of the nonlinear coefficients which again is dependent on the sputtering parameters. Thus for a preferred dot size and growth with time, one would need to strike the right balance between the appropriate choices of material (which influences a, α, ρ, etc.) and sputtering conditions such as ion incidence, temperature, etc., according to the phase diagram of Figs. 1 and 2. Note that there are a few cases with $\varsigma_x > 0$, $\varsigma_y < 0$, $\eta_x < 0$, $\eta_y = 0$ in Figs. 1(b), 1(c), and 2(a); $\varsigma_x \geq 0$, $\varsigma_y \geq 0$, $\eta_x = \eta_y = 0$ in Fig. 2(a); and a few cases of region 12 in Fig. 2(b). These do not appear in the phase diagram because they are not prominent.

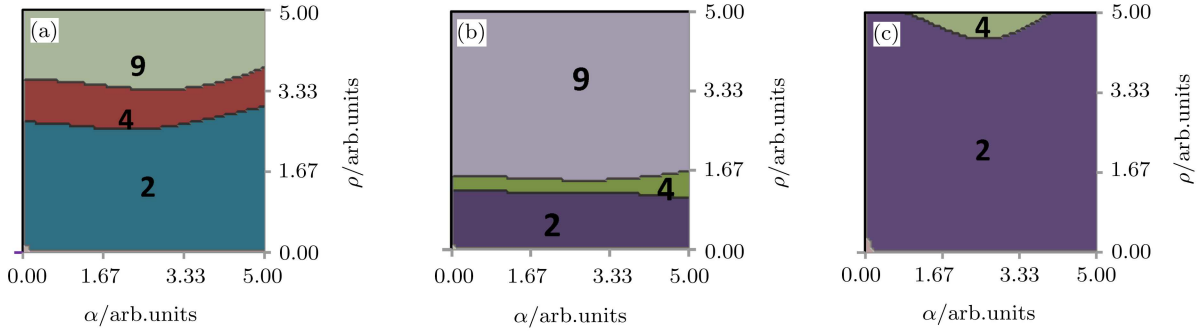

Fig. 1 Phase diagram for $a = 6.0$ and collision cascade parameters α and ρ ranging from 0 to 5. (a) $\theta = 50°$, (b) $\theta = 70°$, (c) $\theta = 30°$. The three regions 2, 4, and 9, are as defined in the text (see also Table 1). (b) and (c) show the boundary shifts in the phase diagram, arising from varying θ for the same parameters as in (a).

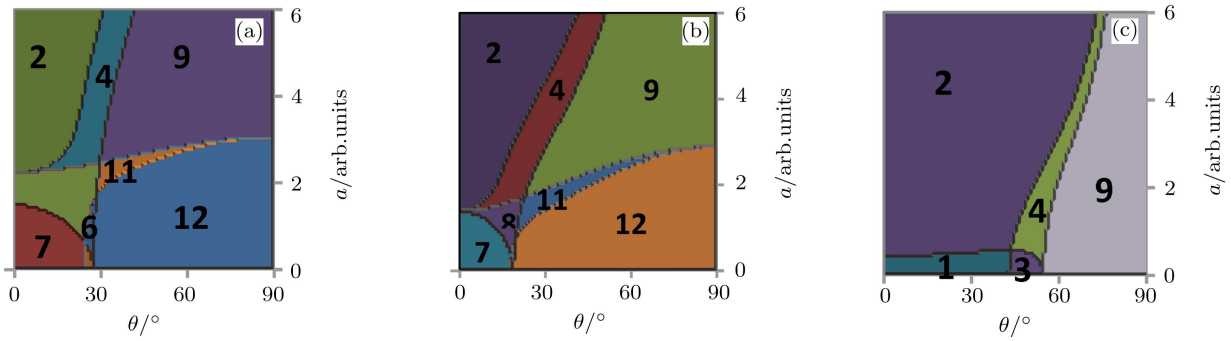

Fig. 2 Phase diagram for the anisotropic cases representative of regions 9, 4, and 2 of Fig. 1(a). (a) $\alpha = 3.3$, $\rho = 4.5$; (b) $\alpha = 1.6$, $\rho = 3.3$; (c) $\alpha = 2.0$, $\rho = 1.0$. The regions found are as labelled in the figure, and defined in the text (see also Table 1).

On the accessibility of some of the regions studied here to probing by experiments, we recall the assumption of the continuum[2,5] and discrete theories[10−11,29−30] that the impinging ion penetrates a distance a into the material, after which it distributes its energy according to a Gaussian distribution, which is a simple representation of the geometry defined by the collision cascades triggered by the impinging ion. Thus, it is possible to design the shape of this geometry through controlled defect creation or doping in the first few surface layers of depth roughly about the penetration depth a. The material and sputtering conditions required to achieve this can be estimated by using the SRIM (stopping and range of ions in matter) simulation package.[16] A comparison of the theoretical parameters with the experimental parameters required to achieve them can be done with this package and has been treated elsewhere.[10−11]

4 Conclusion

Topographic phase diagram calculations over a range of collision cascade parameters of impinging ions in a sputtered surface have been presented. The range, being representative of different distributions of the energy of the impinging ion in the surface, encompasses a variety of sputtering scenarios for different materials. The results revealed a larger number of scaling regimes than previously known. Based on the results presented in this paper and their comparison with existing results, a new interpretation and conceptual framework of the continuum theory has been proposed. This new interpretation explains surface topographies yet unaccounted for and also agrees with the previous interpretation of the theory. This new insight considers the stochastic time evolution equation within the same length scale, thus treating nonlinear effects as an integral part of the sputtering process within this length scale; in contrast to the previous interpretation that considers nonlinear effects as relevant in larger length scales.

Consequently, oblique-incidence nanodot formation has been explained as a result of nonlinear effects counteracting on the ripple formation, and dot size as dependent on the relative magnitudes of the nonlinearities. A possible means of achieving the sputtering parameters necessary for experimental observation of the topographic regions of present interest, e.g. the nano-dot regions, has been discussed. The new scaling regimes found would provide an important focus for further studies as a discretization of the stochastic partial differential equation with coefficients corresponding to the new scaling regimes could be applied in numerical simulations of the surface evolution in order to determine the scaling exponents. Such simulations will constitute an important step in the determination of the scaling exponents for the characterization of sputtered surfaces, most of which are generally unknown.

References

[1] G. Carter, B. Navinsek, and J.L. Whitton, in R. Behrisch (ed.), Topics in Applied Physics, Vol. 52, *Sputtering by Particle Bombardment II*, Springer-Verlag, Heidelberg (1983) p. 140.

[2] R.M. Bradley and J.M. E. Harper, J. Vac. Sci. Technol. **6** (1988) 2390.

[3] E.A. Eklund, R. Bruinsma, J. Rudnick, and R.S. Williams, Phys. Rev. Lett. **67** (1991) 1759.

[4] E. Chason, T.M. Mayer, B.K. Kellerman, D.T. McIlroy, and A.J. Howard, Phys. Rev. Lett. **72** (1994) 3040.

[5] R. Cuerno and A.L. Barabasi, Phys. Rev. Lett. **74** (1995) 4746.

[6] M.A. Makeev, R. Cuerno, and A.L. Barabasi, Nucl Instr and Meth B **97** (2002) 185.

[7] E.O. Yewande, *Modelling and Simulation of Surface Morphology Driven by Ion Bombardment*, Ph.D. thesis, University of Göttingen, Institute for Theoretical Physics, Friedrich Hund Platz 1, Göttingen, Germany (2006).

[8] S. Facsko, T. Dekorsy, C. Koerdt, C. Trappe, H. Kurz, A. Vogt, and H.L. Hartnagel, Science **285** (1999) 1551.

[9] F. Frost, A. Schindler, and F. Bigl, Phys. Rev. Lett. **85** (2000) 4116.

[10] E.O. Yewande, R. Kree, and A.K. Hartmann, Phys. Rev. B **73** (2006) 115434.

[11] E.O. Yewande, R. Kree, and A.K. Hartmann, Phys. Rev. B **75** (2007) 155325.

[12] M. Castro, R. Cuerno, L. Vazquez, and R. Gago, Phys. Rev. Lett. **94** (2005) 016102.

[13] B. Kahng, H. Jeong, and A.L. Barabasi, Appl. Phys. Lett. **78** (2001) 805.

[14] J. Munoz-Garcia, M. Castro, and R. Cuerno, Phys. Rev. Lett. **96** (2006) 086101.

[15] P. Sigmund, Phys. Rev. **184** (1969) 383.

[16] J.F. Ziegler, J.P. Biersack, and U. Littmark, *The Stopping and Range of Ions in Matter*, Pergamon, New York (1985); URL: http://www.srim.org.

[17] R.M. Bradley, Phys. Rev. E **54** (1996) 6149.

[18] F. Frost, Appl. Phys. A: Mater. Sci. Process. **74** (2002) 131.

[19] S. Le Roy, J. Appl. Phys. **106** (2009) 094308.

[20] S. Le Roy, Phys. Rev. B **81** (2010) 161401.

[21] G. Ozaydin, *et al.*, Appl. Phys. Lett. **87** (2005) 163104.

[22] H. Hofsaess and K. Zhang, Appl. Phys. A **92** (2008) 517.

[23] J.A. Sanchez-Garcia, *et al.*, Nanotechnology **19** (2008) 355306.

[24] S. Macko, *et al.*, Nanotechnology **21** (2010) 085301.

[25] J. Zhou, *et al.*, J. Appl. Phys. **109** (2011) 104315.

[26] J. Zhou and M. Lu, Phys. Rev. B **82** (2010) 125404.

[27] A. Keller, *et al.*, Nanotechnology **19** (2008) 135303.

[28] S. Habenicht, W. Bolse, K.P. Lieb, K. Reimann, and U. Geyer, Phys. Rev. B **60** (1999) R2200.

[29] A.K. Hartmann, R. Kree, U. Geyer, and M. Kölbel, Phys. Rev. B **65** (2002) 193403.

[30] E.O. Yewande, A.K. Hartmann, and R. Kree, Phys. Rev. B **71** (2005) 195405.